



Diehl, S. et al. (2020) Extraction of beam-spin asymmetries from the hard exclusive π^+ channel off protons in a wide range of kinematics. *Physical Review Letters*, 125(18), 182001.

There may be differences between this version and the published version. You are advised to consult the publisher's version if you wish to cite from it.

<http://eprints.gla.ac.uk/226672/>

Deposited on: 7 December 2020

Enlighten – Research publications by members of the University of Glasgow
<http://eprints.gla.ac.uk>

Extraction of beam-spin asymmetries from the hard exclusive π^+ channel off protons in a wide range of kinematics

S. Diehl,^{7,24} K. Joo,⁷ A. Kim,⁷ H. Avakian,⁴⁰ P. Kroll,⁴⁹ K. Park,²⁵ D. Riser,⁷ K. Semenov-Tian-Shansky,³⁰ K. Tezgin,⁷ K.P. Adhikari,³³ S. Adhikari,¹² M.J. Amarian,³³ G. Angelini,¹⁴ G. Asryan,⁵⁰ H. Atac,³⁹ L. Barion,¹⁶ M. Battaglieri,^{40,18} I. Bedlinskiy,²⁸ F. Benmokhtar,⁹ A. Bianconi,^{43,21} A.S. Biselli,¹⁰ F. Bossù,⁵ S. Boiarinov,⁴⁰ W.J. Briscoe,¹⁴ W.K. Brooks,^{41,40} D. Bulumulla,³³ V.D. Burkert,⁴⁰ D.S. Carman,⁴⁰ J.C. Carvajal,¹² A. Celentano,¹⁸ P. Chatagnon,²² T. Chetry,²⁷ G. Ciullo,^{16,11} L. Clark,⁴⁴ P.L. Cole,²⁶ M. Contalbrigo,¹⁶ V. Crede,¹³ A. D'Angelo,^{36,19} N. Dashyan,⁵⁰ R. De Vita,¹⁸ M. Defurne,⁵ A. Deur,⁴⁰ C. Dilks,⁸ C. Djalali,^{32,38} R. Dupre,²² H. Egiyan,⁴⁰ M. Ehrhart,¹ A. El Alaoui,⁴¹ L. El Fassi,²⁷ P. Eugenio,¹³ A. Filippi,²⁰ T.A. Forest,¹⁵ Y. Ghandilyan,⁵⁰ G.P. Gilfoyle,³⁵ K.L. Giovanetti,²³ F.X. Girod,⁴⁰ D.I. Glazier,⁴⁴ E. Golovatch,³⁷ R.W. Gothe,³⁸ K.A. Griffioen,⁴⁸ M. Guidal,²² L. Guo,¹² H. Hakobyan,^{41,50} N. Harrison,⁴⁰ M. Hattawy,³³ T.B. Hayward,⁴⁸ D. Heddle,^{6,40} K. Hicks,³² M. Holtrop,²⁹ Y. Ilieva,^{38,14} D.G. Ireland,⁴⁴ B.S. Ishkhanov,³⁷ E.L. Isupov,³⁷ D. Jenkins,⁴⁶ H.S. Jo,²⁵ S. Joosten,¹ D. Keller,⁴⁷ M. Khachatryan,³³ A. Khanal,¹² M. Khandaker,^{31,*} C.W. Kim,¹⁴ W. Kim,²⁵ V. Kubarovskiy,^{40,34} S.E. Kuhn,³³ L. Lanza,¹⁹ M. Leali,^{43,21} P. Lenisa,¹⁶ K. Livingston,⁴⁴ I.J.D. MacGregor,⁴⁴ D. Marchand,²² N. Markov,⁷ L. Marsicano,¹⁸ V. Mascagna,^{42,21} B. McKinnon,⁴⁴ Z.E. Meziani,¹ T. Mineeva,⁴¹ M. Mirazita,¹⁷ V. Mokeev,⁴⁰ C. Munoz Camacho,²² P. Nadel-Turonski,⁴⁰ G. Niculescu,²³ M. Osipenko,¹⁸ M. Paolone,³⁹ L.L. Pappalardo,^{16,11} E. Pasyuk,⁴⁰ W. Phelps,^{6,40} O. Pogorelko,²⁸ J.W. Price,² Y. Prok,^{33,47} B.A. Raue,^{12,40} M. Ripani,¹⁸ A. Rizzo,^{19,36} P. Rossi,^{40,17} J. Rowley,³² F. Sabatié,⁵ C. Salgado,³⁰ A. Schmidt,¹⁴ R.A. Schumacher,⁴ Y.G. Sharabian,⁴⁰ U. Shrestha,³² O. Soto,¹⁷ N. Sparveris,³⁹ S. Stepanyan,⁴⁰ P. Stoler,³⁴ I.I. Strakovsky,¹⁴ S. Strauch,^{38,14} J.A. Tan,²⁵ N. Tyler,³⁸ M. Ungaro,^{40,34} L. Venturelli,^{43,21} H. Voskanyan,⁵⁰ E. Voutier,²² D.P. Watts,⁴⁵ X. Wei,⁴⁰ M.H. Wood,^{3,38} N. Zachariou,⁴⁵ J. Zhang,⁴⁷ and Z.W. Zhao⁸

(The CLAS Collaboration)

¹Argonne National Laboratory, Argonne, Illinois 60439

²California State University, Dominguez Hills, Carson, CA 90747

³Canisius College, Buffalo, NY

⁴Carnegie Mellon University, Pittsburgh, Pennsylvania 15213

⁵IRFU, CEA, Université Paris-Saclay, F-91191 Gif-sur-Yvette, France

⁶Christopher Newport University, Newport News, Virginia 23606

⁷University of Connecticut, Storrs, Connecticut 06269

⁸Duke University, Durham, North Carolina 27708-0305

⁹Duquesne University, 600 Forbes Avenue, Pittsburgh, PA 15282

¹⁰Fairfield University, Fairfield CT 06824

¹¹Università di Ferrara, 44121 Ferrara, Italy

¹²Florida International University, Miami, Florida 33199

¹³Florida State University, Tallahassee, Florida 32306

¹⁴The George Washington University, Washington, DC 20052

¹⁵Idaho State University, Pocatello, Idaho 83209

¹⁶INFN, Sezione di Ferrara, 44100 Ferrara, Italy

¹⁷INFN, Laboratori Nazionali di Frascati, 00044 Frascati, Italy

¹⁸INFN, Sezione di Genova, 16146 Genova, Italy

¹⁹INFN, Sezione di Roma Tor Vergata, 00133 Rome, Italy

²⁰INFN, Sezione di Torino, 10125 Torino, Italy

²¹INFN, Sezione di Pavia, 27100 Pavia, Italy

²²Université Paris-Saclay, CNRS/IN2P3, IJCLab, 91405 Orsay, France

²³James Madison University, Harrisonburg, Virginia 22807

²⁴Justus Liebig University Giessen, 35392 Giessen, Germany

²⁵Kyungpook National University, Daegu 41566, Republic of Korea

²⁶Lamar University, Beaumont, Texas 77705

²⁷Mississippi State University, Mississippi State, MS 39762-5167

²⁸National Research Centre Kurchatov Institute - ITEP, Moscow, 117259, Russia

²⁹University of New Hampshire, Durham, New Hampshire 03824-3568

³⁰Norfolk State University, Norfolk, Virginia 23504

³¹National Research Centre Kurchatov Institute, Petersburg Nuclear Physics Institute, RU-188300 Gatchina, Russia

³²Ohio University, Athens, Ohio 45701

³³Old Dominion University, Norfolk, Virginia 23529

³⁴Rensselaer Polytechnic Institute, Troy, New York 12180-3590

³⁵University of Richmond, Richmond, Virginia 23173

³⁶Universita' di Roma Tor Vergata, 00133 Rome Italy

³⁷Skobeltsyn Institute of Nuclear Physics, Lomonosov Moscow State University, 119234 Moscow, Russia

³⁸University of South Carolina, Columbia, South Carolina 29208

³⁹Temple University, Philadelphia, PA 19122

⁴⁰Thomas Jefferson National Accelerator Facility, Newport News, Virginia 23606

⁴¹Universidad Técnica Federico Santa María, Casilla 110-V Valparaíso, Chile

⁴²Università degli Studi dell'Insubria, 22100 Como, Italy

⁴³Università degli Studi di Brescia, 25123 Brescia, Italy

⁴⁴University of Glasgow, Glasgow G12 8QQ, United Kingdom

⁴⁵University of York, York YO10 5DD, United Kingdom

⁴⁶Virginia Tech, Blacksburg, Virginia 24061-0435

⁴⁷University of Virginia, Charlottesville, Virginia 22901

⁴⁸College of William and Mary, Williamsburg, Virginia 23187-8795

⁴⁹Fachbereich Physik, Universität Wuppertal, D-42097 Wuppertal, Germany

⁵⁰Yerevan Physics Institute, 375036 Yerevan, Armenia

We have measured beam-spin asymmetries to extract the $\sin\phi$ moment $A_{LU}^{\sin\phi}$ from the hard exclusive $\bar{e}p \rightarrow e'n\pi^+$ reaction above the resonance region, for the first time with nearly full coverage from forward to backward angles in the center-of-mass. The $A_{LU}^{\sin\phi}$ moment has been measured up to 6.6 GeV^2 in $-t$, covering the kinematic regimes of Generalized Parton Distributions (GPD) and baryon-to-meson Transition Distribution Amplitudes (TDA) at the same time. The experimental results in very forward kinematics demonstrate the sensitivity to chiral-odd and chiral-even GPDs. In very backward kinematics where the TDA framework is applicable, we found $A_{LU}^{\sin\phi}$ to be negative, while a sign change was observed near 90° in the center-of-mass. The unique results presented in this paper will provide critical constraints to establish reaction mechanisms that can help to further develop the GPD and TDA frameworks.

PACS numbers: 13.60.Le, 14.20.Dh, 14.40.Be, 24.85.+p

Hard exclusive pseudoscalar meson electroproduction processes offer a unique opportunity to study the structure of the nucleon. They allow one to vary the size of both the probe (i.e. the photon virtuality Q^2) and the target (the four-momentum transfer to the nucleon (meson) t (u)). These reactions reveal rich information about the structure of the nucleon and the reaction dynamics.

At very forward kinematics ($-t/Q^2 \ll 1$) where the Bjorken limit is applicable, hard exclusive pseudoscalar meson electroproduction can be factorized into a perturbatively calculable hard sub-process at the quark level, $\gamma^*q \rightarrow \pi q$, and the hadronic matrix elements which are expressed via the leading twist Generalized Parton Distributions (GPDs) of the nucleon and the pion Distribution Amplitude (DA) [1-3] as shown in Fig. 1 (a). GPDs are light-cone matrix elements that can be expressed as non-local bilinear quark and gluon operators that describe the transition from the initial to the final nucleon and reveal the 3-dimensional structure of the nucleon at the parton level by correlating the internal transverse position of the partons to their longitudinal momentum [4-6]. A first experimental confirmation of the applicability of the leading twist GPD framework was provided by deeply virtual Compton scattering (DVCS) experiments at Jefferson Lab (JLab), DESY and CERN (see, e.g., [7-12]).

While the DVCS process gives access to all chiral-even GPDs H , \tilde{H} , E and \tilde{E} , pseudoscalar meson production is especially helpful in probing the polarized GPDs (\tilde{H} and \tilde{E}), which contain information about the spatial distribution of the quark spin [13, 14]. However, extensive

experimental [15-29] and theoretical [2, 3, 30-32] investigations of hard exclusive pseudoscalar meson electroproduction in recent years have shown that the asymptotic leading-twist approximation is not readily applicable in the range of kinematics accessible to current experiments. In fact, there are strong contributions from transversely polarized virtual photons that are asymptotically suppressed by $1/Q^2$ in the cross sections and have to be considered by introducing chiral-odd GPDs (H_T , \tilde{H}_T , E_T , and \tilde{E}_T) into the framework. For instance for π^0 and η electroproduction, the contributions from transversely polarized virtual photons are significant and the introduction of chiral-odd GPDs is needed to reproduce the measured cross sections as well as large beam- and target-spin asymmetries with GPD models [2, 3, 21, 23, 24, 28, 33, 34].

A further generalization of the GPD concept has been introduced for non-diagonal transitions where the initial and final states are hadronic states of different baryon number [35-38]. In very backward kinematics ($-u/Q^2 \ll 1$) the collinear factorized description can be applied in terms of a convolution of a hard part calculable in perturbative QCD, and the soft parts expressed in terms of nucleon-to-pion baryonic Transition Distribution Amplitudes (TDAs) and the nucleon DA as shown in Fig. 1 (b). Like GPDs, nucleon-to-meson TDAs are defined through hadronic matrix elements of non-local three-quark light-cone operators. Nucleon-to-meson TDAs are universal functions that parameterize the non-perturbative structure of hadrons. Within

the reaction mechanism involving TDAs, the three-quark core of the target nucleon absorbs most of the virtual photon momentum and recoils forward, while a pion from the mesonic cloud of the nucleon remains with a low momentum heading backward. Therefore, the process brings a bulk of new information on hadronic structure and can be used *e.g.* to probe the non-minimal Fock components of hadronic light-cone wave functions. In contrast to the very forward kinematic regime in the Bjorken limit, the contribution of the transversely polarized virtual photon exchange is expected to dominate the process to leading twist-3 accuracy in very backward kinematics. Recent publications on exclusive π^+ electroproduction by the CLAS collaboration [39] and on ω electroproduction from JLab Hall C [40] in very backward kinematics have shown a first indication of the applicability of the TDA model to predict the magnitude and the scaling behavior of the cross section, as well as the dominance of the transverse over the longitudinal cross section at sufficiently large Q^2 in the backward regime.

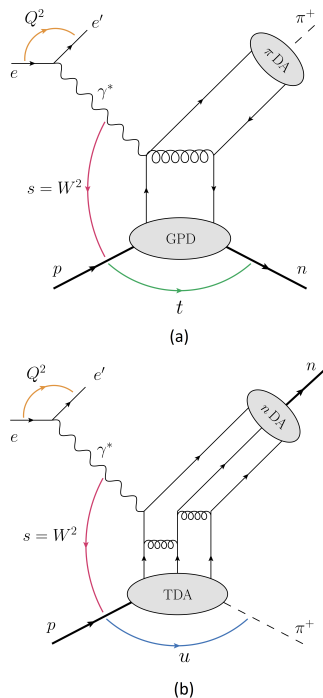


FIG. 1: (a) Exclusive electroproduction of a pion on the proton in very forward kinematics ($-t/Q^2 \ll 1$), described by GPDs [2, 3]. (b) Factorization of the same reaction in very backward kinematics ($-u/Q^2 \ll 1$), described by TDAs [39, 46].

The GPD and TDA approaches describe complementary kinematic domains. While GPDs are applicable for small $-t$, TDAs can be applied for small $-u$, corresponding to large $-t$. Although these two approaches deal with domains that are well distinct at asymptotic energies, they are not well separated in the kinematic range acces-

sible to current experiments. Therefore, it is important to investigate in detail the phenomenological differences of the two approaches over a large range of momentum transfer t . In previous publications, *e.g.* [27, 39], only very limited kinematic regions covering either the GPD or the TDA regime exclusively have been investigated. In this letter, we present a measurement of the beam-spin asymmetries (BSA) for the hard exclusive electroproduction $ep \rightarrow e'n\pi^+$ for full π^+ center-of-mass (CM) angular coverage with a large range of t or u .

GPDs and TDAs can be accessed through different observables in exclusive meson production, such as differential cross sections and beam and target polarization asymmetries [41, 42]. The focus of this work is on the extraction of the $A_{LU}^{\sin\phi}$ moment from the beam-spin asymmetry. The beam-spin asymmetry in the one-photon exchange approximation is defined as follows [41]:

$$BSA(t, \phi, x_B, Q^2) = \frac{d\sigma^+ - d\sigma^-}{d\sigma^+ + d\sigma^-} = \frac{A_{LU}^{\sin\phi} \sin\phi}{1 + A_{UU}^{\cos\phi} \cos\phi + A_{UU}^{\cos 2\phi} \cos 2\phi}, \quad (1)$$

where $d\sigma^\pm$ is the differential cross section for each beam helicity state (\pm). For the positive / negative helicity the spin is parallel / anti-parallel to the beam direction. The subscripts ij represent the longitudinal (L) or unpolarized (U) state of the beam and the target, respectively. ϕ is the azimuthal angle between the electron scattering plane and the hadronic reaction plane.

Due to the interference between the amplitudes for longitudinal (γ_L^*) and transverse (γ_T^*) virtual photon polarizations, the moment $A_{LU}^{\sin\phi}$ is proportional to the polarized structure function $\sigma_{LT'}$ [41]:

$$A_{LU}^{\sin\phi} = \frac{\sqrt{2\epsilon(1-\epsilon)} \sigma_{LT'}}{\sigma_T + \epsilon\sigma_L}, \quad (2)$$

where the structure functions σ_L and σ_T correspond to longitudinal and transverse virtual photons, and ϵ describes the ratio of their fluxes.

Hard exclusive π^+ electroproduction was measured at Jefferson Lab with the CEBAF Large Acceptance Spectrometer (CLAS) [43]. Beam-spin asymmetries were extracted over a wide range in Q^2 , t , x_B and ϕ . The incident electron beam was longitudinally polarized and had an energy of 5.498 GeV. The target was unpolarized liquid hydrogen. The CLAS detector consisted of six identical sectors within a toroidal magnetic field. The momentum and the charge polarity of the particles were determined by 3 regions of drift chambers from the curvature of the particle trajectories in the magnetic field. The electron identification was based on a lead-scintillator electromagnetic sampling calorimeter in combination with a Cherenkov counter. For the selection of deeply inelastic scattered electrons, cuts on $Q^2 > 1 \text{ GeV}^2$ and on the

invariant mass of the hadronic final state $W > 2$ GeV were applied. Positive pions were identified by time-of-flight measurements. To select the exclusive $e'\pi^+n$ final state, events with exactly one electron and one π^+ were detected, and a cut around the neutron peak in the missing mass spectrum was performed. The mean signal-to-background ratio in the forward region is 15.3, while it decreases to 4.9 in the backward region.

Beam-spin asymmetries (BSA) were measured in the Q^2 range from 1 to 4.6 GeV², $-t$ up to 6.6 GeV² and x_B from 0.1 - 0.6. The BSA and its statistical uncertainty were determined experimentally from the number of counts with positive and negative helicity (N_i^\pm), in a specific bin i as:

$$BSA = \frac{1}{P_b} \frac{N_i^+ - N_i^-}{N_i^+ + N_i^-}, \quad \sigma_{BSA} = \frac{2}{P_b} \sqrt{\frac{N_i^+ N_i^-}{(N_i^+ + N_i^-)^3}}, \quad (3)$$

where P_b is the average magnitude of the beam polarization. P_b was measured with a Møller polarimeter upstream of CLAS and was $74.9 \pm 2.4\%$ (stat.) $\pm 3.0\%$ (sys.).

To extract the $\sin\phi$ moment $A_{LU}^{\sin\phi}$, the beam-spin asymmetry was measured as a function of the azimuthal angle ϕ . Then a fit of the data with the functional form shown in Eq. (1) was applied. Figure 2 shows the beam-spin asymmetry as a function of ϕ for events in the forward and backward regions, integrated over all other kinematic variables. Experimentally the forward region is defined as $\cos\theta_{CM} > 0$ and $-t < 1.5$ GeV², while the backward region is defined by a cut on $\cos\theta_{CM} < 0$ and $-u < 2.0$ GeV², where θ_{CM} is the polar angle of the pion in the frame boosted along the momentum transfer \vec{q} direction. As expected the ϕ -dependence can be

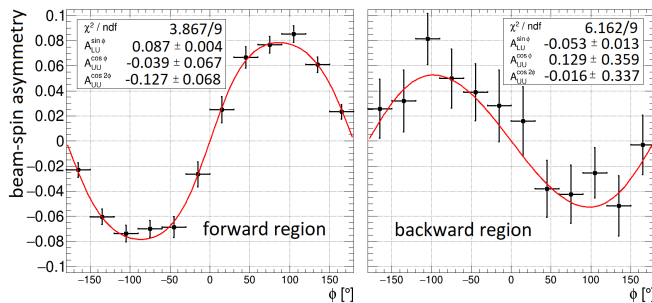


FIG. 2: Beam-spin asymmetry as a function of ϕ for π^+ emitted in the forward (left) and backward (right) regions, integrated over all other kinematic variables. The vertical error bars show the statistical uncertainty of each point, while the horizontal bars correspond to the bin width. The red line shows the fit with the functional form of Eq. (1).

well described by Eq. (1). The asymmetry of the background has been extracted with the side-band method by selecting a missing-mass interval on the right side of the missing neutron peak. These events represent the

background under the region of interest and therefore its asymmetry has to be subtracted. The amplitude of the background asymmetry has been determined in the same way as for the exclusive events, with a $\sin\phi$ fit of the ϕ -dependence of the BSA. The $\sin\phi$ amplitude of the background is 0.032 ± 0.006 in the forward region and decreases to 0.00 ± 0.01 in the backward region. Based on the signal-to-background ratio determined from a fit of the missing mass spectrum in each kinematic bin, a bin-by-bin background subtraction has been performed for the extracted $A_{LU}^{\sin\phi}$ values.

Several sources of systematic uncertainty were investigated, including particle identification, background subtraction, beam polarization, and the influence of the $A_{UU}^{\cos\phi}$ and $A_{UU}^{\cos 2\phi}$ moments. The correlation between the unpolarized moments and $A_{LU}^{\sin\phi}$ was found to be very small. The systematic uncertainty for each contribution was determined by a variation of the contributing source around its nominal value. To estimate the impact of acceptance effects, a Monte Carlo simulation which included a parametrization of the kinematic behaviour following that of the actual data was performed. The impact of acceptance effects turned out to be small and is included in the systematic uncertainty. The total systematic uncertainty in each bin is defined as the square-root of the quadratic sum of the uncertainties from all sources. It has been found to be comparable to the statistical uncertainty.

Figure 3 shows the results for $A_{LU}^{\sin\phi}$ in the region of $-t$ up to 0.75 GeV² ($-t/Q^2 \approx 0.25$) where the leading-twist GPD framework is applicable and compares them to the theoretical predictions from the GPD-based model by Goloskokov and Kroll (GK) [44]. The experimental data is binned in $-t$ and integrated over the complete Q^2 distribution ranging from 1.0 to 4.5 GeV² and x_B ranging from 0.1 to 0.6. The band on the theoretical prediction represents the range in Q^2 and x_B accessible with our measurements. The GK model includes chiral-odd GPDs to calculate the contributions from the transversely polarized virtual photon amplitudes, with their t -dependence incorporated from Regge phenomenology. The GPDs are constructed from double distributions and constrained by results from lattice QCD and transversity parton distribution functions [44]. A special emphasis is given to the GPDs H_T and $\bar{E}_T = 2\tilde{H}_T + E_T$, while contributions from other chiral-odd GPDs are neglected in the calculations, unlike chiral-even GPDs, where some contributions are negligible but still included. The pion pole contribution to the amplitudes is taken into account for both the longitudinally and transversely polarized virtual photons. However, its contribution to the transversely polarized virtual photon amplitudes is very small.

The magnitude of $A_{LU}^{\sin\phi}$ (see Eq. (2)) is proportional to the ratio of the interference structure function $\sigma_{LT'}$ and the unseparated cross section $\sigma_0 = \sigma_T + \epsilon\sigma_L$, where σ_0

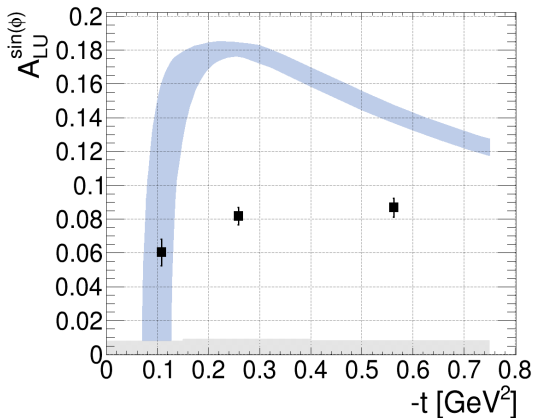


FIG. 3: $A_{LU}^{\sin\phi}$ (black rectangles) as a function of $-t$ in the forward kinematic regime and their systematic uncertainty (grey bins). For comparison the theoretical prediction from the GPD-based Goloskokov-Kroll model (blue band) is shown. The band of the theoretical prediction corresponds to the range accessible with our measurements in Q^2 and x_B .

is forward peaked due to the pion pole term contribution and $\sigma_{LT'}$ is constrained to be zero at $t = t_{min}$ ($\theta_{CM} = 0$) due to angular momentum conservation. $\sigma_{LT'}$ can be expressed through the convolutions of GPDs with subprocess amplitudes (twist-2 for the longitudinal and twist-3 for the transverse amplitudes) and contains the products of chiral-odd and chiral-even terms [2]:

$$\sigma_{LT'} \sim \text{Im} \left[\langle \bar{E}_{T-eff} \rangle^* \langle \tilde{H}_{eff} \rangle + \langle H_{T-eff} \rangle^* \langle \tilde{E}_{eff} \rangle \right], \quad (4)$$

where all involved GPDs are influenced directly or indirectly by the pion pole term, for example:

$$\tilde{E}_{eff} = \tilde{E} + \text{pole term}, \quad (5)$$

$$\tilde{H}_{eff} = \tilde{H} + \frac{\xi^2}{1 - \xi^2} \tilde{E}_{eff}, \quad (6)$$

with the skewness $\xi \sim x_B/(2 - x_B)$. For π^+ the imaginary part of small chiral-odd GPDs in $\sigma_{LT'}$ is significantly amplified by the pion pole term, which is real and exactly calculable. This feature increases the sensitivity of polarized observables to chiral-odd GPDs in contrast to the π^0 and η channels where the pole contribution is not present. In the GK model $\sigma_{LT'}$ is dominated by $\text{Im}[\langle H_{T-eff} \rangle^* \langle \tilde{E}_{eff} \rangle]$ and \tilde{E}_{eff} is dominated by the pion pole term, while other GPD products are considered to be negligible.

The comparison between the experimental results and the theoretical predictions shows that the magnitude of the GK model calculations is overestimated and the t -dependence of the measured $A_{LU}^{\sin\phi}$ values shows a much flatter slope than the predicted curve. The discrepancy in magnitude and t -dependence might be due to the interplay of the pion pole term with the poorly known chiral-odd GPDs H_T and \bar{E}_T . Even though previous studies

showed that the GPD model can be well applied to predict π^0 and η cross sections [20, 21, 23], the results in Fig. 3 show that the GPDs and the model have to be tuned to describe BSA as well. While the beam-spin asymmetry calculations for the π^+ channel are overestimated by the GK model, the absence of the pion pole term in case of the π^0 and η channels leads to a significantly smaller predicted beam-spin asymmetry by the GK model, which underestimates the experimental observation as shown in Ref. [28]. The combined analysis of these unique π^+ data with the π^0 and η channels [16, 20, 21, 23, 28] can be performed to significantly constrain these poorly known GPDs.

While the framework of GPDs is only applicable in very forward kinematics, a complete understanding of the reaction mechanism requires measurements over the complete range of $-t$. As shown in Fig. 4 we extended the kinematic region for the extraction of $A_{LU}^{\sin\phi}$ up to $-t = 6.6 \text{ GeV}^2$, which is close to the maximal accessible $-t$ value. The data are binned in $-t$ and integrated over the complete Q^2 distribution ranging from $1 \text{ GeV}^2 - 4.5 \text{ GeV}^2$ and x_B ranging from 0.1 to 0.6.

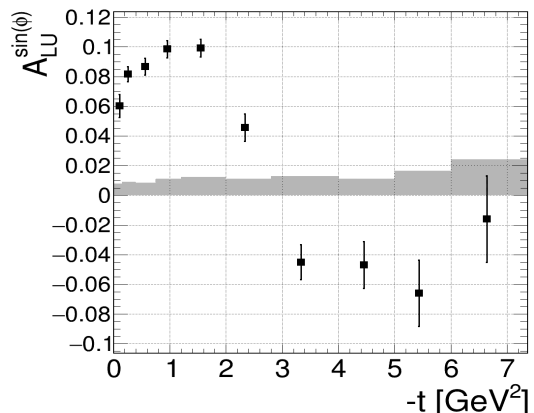


FIG. 4: $A_{LU}^{\sin\phi}$ as function of $-t$. The shaded area represents the systematic uncertainty.

The sign of $A_{LU}^{\sin\phi}$ in forward kinematics is clearly positive, which is confirmed by the most recent GPD models [44], while in backward kinematics a clearly negative sign is observed. Large t corresponds to small u , so that at backward angles the u channel dominates (Fig. 1 (b)). Thus it is expected that the TDA-based framework can be applied in very backward kinematics.

Similarly to Eq. (4) for very forward kinematics, $\sigma_{LT'}$ in the backward regime can be expressed through the interference between the leading twist transverse amplitude of the convolution in terms of twist-3 πN TDAs (H^{tw3}) and nucleon DAs (ϕ^{tw3}) and the next leading sub-process longitudinal amplitude of the convolution involving twist-4 TDAs (H^{tw4}) and DAs (ϕ^{tw4}) [46-48]:

$$\sigma_{LT'} \sim \text{Im} \left[\langle H_i^{tw3} \phi_j^{tw3} \rangle (\langle H_i^{tw4} \phi_j^{tw3} \rangle + \langle H_i^{tw3} \phi_j^{tw4} \rangle)^* \right]. \quad (7)$$

A complete theoretical study of this twist-4 longitudinal amplitude is not yet available, and it is an open question which particular twist-4 πN TDAs and DAs will contribute to the BSA and what kind of phenomenological models can be implemented for these quantities. Nevertheless, our measurement will significantly constrain the nearly unknown TDAs and help to further develop the TDA-based framework.

Also, for the intermediate kinematic region around $\theta_{CM} = 90^\circ$, first models have been introduced [49, 50]. However, calculations exist only for wide-angle Compton scattering [49] and the photoproduction of pions [50]. Nevertheless, the introduced concepts can also be applied to electroproduction and will help to connect the GPD and TDA kinematic regimes in the future.

As shown in Fig. 4, the t -dependence of $A_{LU}^{\sin\phi}$ makes a clear transition from positive values with a maximum value of 0.10 in the forward region to negative values down to a minimum value of -0.06 in the backward region. The sign change occurs around $-t = 3 \text{ GeV}^2$, which corresponds to $\theta_{CM} = 90^\circ$, and marks the transition between the π^+ emitted in the forward and backward directions. Therefore, the sign change may be interpreted as an indication for a transition between the GPD and TDA regimes. The wide range of kinematics presented in this work will also enable the development of a more consistent reaction mechanism for the intermediate kinematical regime in-between the very forward regime with GPD-based description and the very backward regime with description in terms of TDAs.

Figure 5 shows $A_{LU}^{\sin\phi}$ as a function of Q^2 , integrated over x_B in the top plots and as a function of x_B , integrated over Q^2 in the bottom plots, for pions going in the forward (left) and backward (right) regions, as defined earlier. The figure clearly shows that the sign change between the forward and the backward region is present for all Q^2 - and x_B -bins. In the forward region, the Q^2 -dependence shows a rather flat behavior, while $A_{LU}^{\sin\phi}$ rises for small x_B until it reaches a constant level for $x_B > 0.26$. In the backward region the Q^2 - and x_B -dependencies show a rather flat behavior. However, the effect is not statistically significant.

In summary, we have measured for the first time the $\sin\phi$ moment $A_{LU}^{\sin\phi}$ of beam-spin asymmetries for $\vec{e}p \rightarrow e'n\pi^+$ at large photon virtuality, above the resonance region over the full range of polar angles θ_{CM} that cover the complete kinematic region of the GPD and TDA frameworks simultaneously. A comparison in very forward kinematics showed that our $A_{LU}^{\sin\phi}$ measurement cannot be described in magnitude or t -dependence by the most advanced GPD-based model [44]. In very forward kinematics where the GPD framework is applicable, we measure clearly positive values of $A_{LU}^{\sin\phi}$, while in very backward kinematics where the TDA framework is applicable, negative $A_{LU}^{\sin\phi}$ values have been measured. A clear sign change of $A_{LU}^{\sin\phi}$ has been observed around

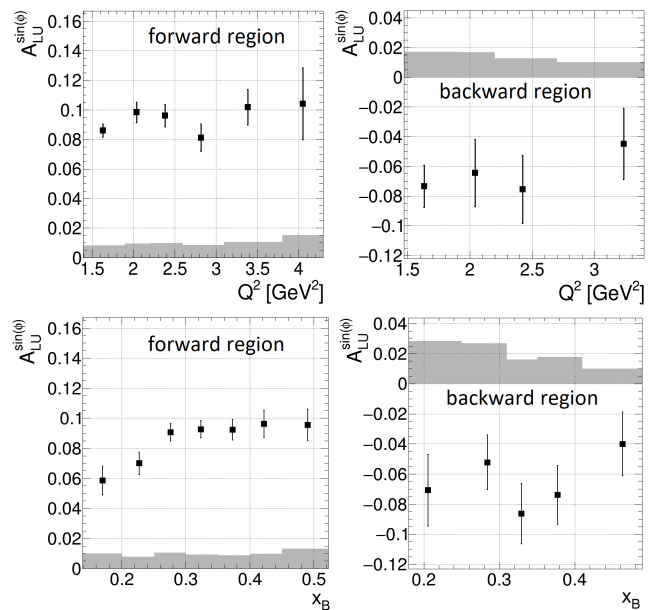


FIG. 5: $A_{LU}^{\sin\phi}$ as function of Q^2 (top) and x_B (bottom) for pions going in the forward (left) and backward (right) regions. The shaded area represents the systematic uncertainty.

$\theta_{CM} = 90^\circ$. The presented data provide important constraints for the development of a reaction mechanism that describes the complete kinematic regime including GPDs and TDAs as well as the intermediate regime. To obtain a deeper understanding, and to reveal more details of the reaction mechanism, measurements with a higher precision and over a larger range of Q^2 will be performed with the upgraded 12 GeV CEBAF accelerator at JLab and in the crossed reaction $\bar{N}N \rightarrow \gamma^*\pi$, accessible with PANDA at FAIR [51–53] and $\pi N \rightarrow N\gamma^*$ or $\pi N \rightarrow NJ/\Psi$ at JPARC [54]. The data-set presented in this work can be downloaded from Ref. [45].

We acknowledge the outstanding efforts of the staff of the Accelerator and the Physics Divisions at Jefferson Lab in making this experiment possible. We also acknowledge very helpful discussions with L. Szymanowski and B. Pire. This work was supported in part by the U.S. Department of Energy, the National Science Foundation (NSF), the Italian Istituto Nazionale di Fisica Nucleare (INFN), the French Centre National de la Recherche Scientifique (CNRS), the French Commissariat pour l’Energie Atomique, the UK Science and Technology Facilities Council, and the National Research Foundation (NRF) of Korea. The Southeastern Universities Research Association (SURA) operates the Thomas Jefferson National Accelerator Facility for the US Department of Energy under Contract No. DE-AC05-06OR23177. The work is also supported in part by DOE grant no: DE-FG02-04ER41309.

-
- * Current address: Idaho State University, Pocatello, Idaho 83209
- † Current address: Università degli Studi di Brescia, 25123 Brescia, Italy
- [1] J. C. Collins, L. Frankfurt and M. Strikman, *Phys. Rev. D* **56**, 2982 (1997).
- [2] S. V. Goloskokov and P. Kroll, *Eur. Phys. J. A* **47**, 112 (2011).
- [3] G. R. Goldstein, J. O. Hernandez and S. Liuti, *Phys. Rev. D* **91**, 114013 (2015).
- [4] D. Müller et al., *Fortsch. Phys.* **42**, 101 (1994).
- [5] A. V. Radyushkin, *Phys. Lett. B* **380**, 417 (1996).
- [6] X. Ji, *Phys. Rev. Lett.* **78**, 610 (1997).
- [7] C. Muñoz Camacho et al. (*Jefferson Lab Hall A Collaboration*), *Phys. Rev. Lett.* **97**, 262002 (2006).
- [8] F. X. Girod et al. (*CLAS Collaboration*), *Phys. Rev. Lett.* **100**, 162002 (2008).
- [9] A. Airapetian et al. (*HERMES Collaboration*), *JHEP* **11**, 08 (2009).
- [10] F. D. Aaron et al. (*H1 Collaboration*), *Phys. Lett. B* **681**, 391 (2009).
- [11] S. Chekanov et al. (*ZEUS Collaboration*), *J. High Energy Phys.* **05**, 108 (2009).
- [12] R. R. Akhunzyanov et al. (*COMPASS Collaboration*), *Phys. Lett. B* **793**, 188 (2019).
- [13] K. Goecke et al., *Prog. Part. Nucl. Phys. A* **47**, 401 (2001).
- [14] R. Jakob et al., *J. Phys. G* **22**, 45 (1996).
- [15] A. Airapetian et al. (*HERMES Collaboration*), *Phys. Lett. B* **535**, 85 (2002).
- [16] R. De Masi et al. (*CLAS Collaboration*), *Phys. Rev. C* **77**, 042201 (2008).
- [17] A. Airapetian et al. (*HERMES Collaboration*), *Phys. Lett. B* **659**, 486 (2008).
- [18] A. Airapetian et al. (*HERMES Collaboration*), *Phys. Lett. B* **682**, 345 (2010).
- [19] E. Fuchey et al. (*Hall A DVCS Collaboration*), *Phys. Rev. C* **83**, 025201 (2011).
- [20] I. Bedlinskiy et al. (*CLAS Collaboration*), *Phys. Rev. Lett.* **109**, 112001 (2012).
- [21] I. Bedlinskiy et al. (*CLAS Collaboration*), *Phys. Rev. C* **90**, 025205 (2014).
- [22] M. Defurne et al. (*Hall A DVCS Collaboration*), *Phys. Rev. Lett.* **117**, 262001 (2016).
- [23] I. Bedlinskiy et al. (*CLAS Collaboration*), *Phys. Rev. C* **95**, 035202 (2017).
- [24] A. Kim et al. (*CLAS Collaboration*), *Phys. Lett. B* **768**, 168 (2017).
- [25] P. Bosted et al. (*CLAS Collaboration*), *Phys. Rev. C* **95**, 035207 (2017).
- [26] M. Mazouz et al. (*Hall A DVCS Collaboration*), *Phys. Rev. Lett.* **118**, 222002 (2017).
- [27] P. Bosted et al. (*CLAS Collaboration*), *Phys. Rev. C* **95**, 035206 (2017).
- [28] B. Zhao et al. (*CLAS Collaboration*), *Phys. Lett. B* **789**, 426 (2019).
- [29] M. G. Alexeev et al. (*COMPASS Collaboration*), *Phys. Lett. B* **805**, 135454 (2020).
- [30] M. Diehl and W. Kugler, *Eur. Phys. J. C* **52**, 933 (2007).
- [31] G. Duplančić, D. Mller and K. Passek-Kumerički, *Phys. Lett. B* **771**, 603 (2017).
- [32] M. Siddikov and I. Schmidt, *Phys. Rev. D* **99**, 116005 (2019).
- [33] S. Ahmad, G. R. Goldstein and S. Liuti, *Phys. Rev. D* **79**, 054014 (2009).
- [34] G. R. Goldstein, J. O. Hernandez and S. Liuti, *Phys. Rev. D* **84**, 034007 (2011).
- [35] L. L. Frankfurt, P. V. Pobylitsa, M. V. Polyakov and M. Strikman, *Phys. Rev. D* **60**, 014010 (1999).
- [36] B. Pire and L. Szymanowski, *Phys. Lett. B* **622**, 83 (2005).
- [37] B. Pire and L. Szymanowski, *Phys. Rev. D* **71**, 111501(R) (2005).
- [38] J. P. Lansberg, B. Pire and L. Szymanowski, *Phys. Rev. D* **75**, 074004 (2007).
- [39] K. Park et al. (*CLAS Collaboration*), *Phys. Lett. B* **780**, 340 (2018).
- [40] W. B. Li et al. (*Jefferson Lab F_π Collaboration*), *Phys. Rev. Lett.* **123**, 182501 (2019).
- [41] D. Drechsel and L. Tiator, *J. Phys. G* **18**, 449 (1992).
- [42] M. Diehl and S. Sapeta, *Eur. Phys. J. C* **41**, 515 (2005).
- [43] B. A. Mecking et al. (*CLAS Collaboration*), *Nucl. Instr. Meth. A* **503**, 513 (2003).
- [44] S. V. Goloskokov and P. Kroll, *Eur. Phys. J. C* **65**, 137 (2010).
- [45] CLAS physics database, <https://clas.sinp.msu.ru/cgi-bin/jlab/db.cgi>.
- [46] J. P. Lansberg, B. Pire, K. Semenov-Tian-Shansky and L. Szymanowski, *Phys. Rev. D* **85**, 054021 (2012).
- [47] V. M. Braun, S. E. Derkachov, G. Korchemsky and A. Manashov, *Nucl. Phys. B* **553**, 355 (1999).
- [48] V. Braun, R. Fries, N. Mahnke and E. Stein, *Nucl. Phys. B* **589**, 381 (2000).
- [49] M. Diehl and P. Kroll, *Eur. Phys. J. C* **73**, 2397 (2013).
- [50] P. Kroll and K. Passek-Kumericki, *Phys. Rev. D* **97**, 074023 (2018).
- [51] J. P. Lansberg, B. Pire, K. Semenov-Tian-Shansky and L. Szymanowski, *Phys. Rev. D* **86**, 114033 (2012).
- [52] J. P. Lansberg, B. Pire, K. Semenov-Tian-Shansky and L. Szymanowski, *Phys. Rev. D* **87**, 059902(E) (2013).
- [53] B. Pire et al., *Phys. Lett. B* **724**, 99 (2013). Erratum: *Phys. Lett. B* **764**, 335 (2017).
- [54] B. P. Singh et al. (*The PANDA Collaboration*), *Eur. Phys. J. A* **51**, 107 (2015).
- [55] T. Sawada, W. C. Chang, S. Kumano, J. C. Peng, S. Sawada and K. Tanaka, *Phys. Rev. D* **93**, 114034 (2016).